17th Australasian Wind Engineering Society Workshop
Wellington, New Zealand
12-13 February 2015

Wind effects on parabolic trough collectors at different positions in the solar field

J. Paetzold[1], S. Cochard[1], D.F. Fletcher[2], and A. Vassallo[2]

[1]School of Civil Engineering, Faculty of Engineering and IT
The University of Sydney, New South Wales 2006, Australia

[2]School of Chemical and Biomolecular Engineering, Faculty of Engineering and IT
The University of Sydney, New South Wales 2006, Australia

Abstract

The airflow around parabolic trough solar collectors in a solar field is simulated with Computational Fluid Dynamics (CFD) tools. The results of steady-state simulations of two different trough geometries, a deep and a shallow one, are compared in this study at the level of the solar field at a particular orientation of the trough. For the shallow trough geometry initial data from a transient periodic simulation are also presented. It is shown that the aerodynamic loads on the troughs in the centre of a solar field of a parabolic (PTC) power plant are significantly lower than those on an individual collector row and those in the first row of the field. The first row is the only one subjected directly to the atmospheric boundary layer flow, while the following rows experience highly turbulent flow conditions from the wake of the upstream collectors. Therefore, the highest forces and pitching moments were experienced in the first row, which were almost identical to those for a single row. A deep trough experiences higher loads than a shallow one at the level of a single row and in the first few rows of the solar field. However, there is hardly any difference in the aerodynamic loads between deep and shallow trough from the fourth row onwards.

Introduction

Parabolic trough power plants are often located in areas that are subjected to high wind speeds, as an open terrain without any obstructions is beneficial for the plant performance. The wind impacts both the structural requirements and the performance of the plant. The aerodynamic loads from the wind impose strong requirements on the support structure of the reflectors, and they also impact the tracking accuracy. On a thermal level the airflow around the glass envelope of the receiver tube cools its outer surface through forced convection, thereby contributing to the heat loss.

Previous studies of the wind effects on parabolic troughs mostly focused on one particular trough geometry (e.g. Hachicha et al., 2013; Hosoya et al., 2008; Naeeni and Yaghoubi, 2007), usually idealised to a continuous parabolic shape. Sun et al. (2014) provided a summary and review of the published research about wind loads on parabolic troughs and heliostats. Earlier work by the authors found that the aerodynamic loads on a deep trough with a short focal length are higher than the loads on a shallow trough with a longer focal length, while the deep trough reduces the heat loss due to forced convection (Paetzold et al., 2014).

Peterka et al. (1980) performed experiments in a wind tunnel on individual troughs with different focal lengths, and they extended their studies also to the level of the full solar field at small model scale for a shallow trough geometry. They found that the aerodynamic loads significantly reduce in the collector rows further downwind in the field. Already in the second row the loads were notably lower than in the most upwind collectors. In varying the gap spacing between the individual PTCs, no significant change in the loads was experienced, while a change in the spacing between collector rows slightly changed the loads in some configurations. The experiments on a similar scale of Hosoya et al. (2008) confirmed the results of significantly lower loads in the downwind rows of collectors in the solar field. From the fifth row onwards the aerodynamic loads experienced in the experiments were virtually constant. In a numerical study investigating the wind flow around a solar field Mier-Torrecilla et al. (2014) confirmed the trend of the wind loads reducing significantly in the interior of the field. They highlighted the importance of transient simulations in order to be able to comprehensively analyse the effect of the wind on the solar field. According to Hosoya et al. (2008) a position in the interior part of the field from the 5th row and the 4th column from the edge represent the majority of the collectors in a realistic solar field.

This study analyses the wind effects in a full-scale solar field of the shallow and the deep trough as analysed on the level of a single row by Paetzold et al. (2014). A large domain with 8 rows of parabolic collectors is simulated at full scale in steady-state simulations in an atmospheric boundary layer flow. The effect of the wake of a collector row on the following collectors is analysed, and the aerodynamic loads are compared between the two geometries.

Methodology

The simulation approach for the present work is similar to that presented in Paetzold et al. (2014). Three-dimensional numerical simulations using the commercial CFD software ANSYS® CFX 15.0 were conducted on troughs with two different focal lengths of the parabola, i.e. the deep trough with a focal length of 1/5 of the trough aperture and the shallow trough with a focal length of 1/3 of the trough aperture. The troughs were oriented in a way that the concave opening of the trough was rotated into the wind at a pitch angle of 45° (with 0° being an upward facing position). This orientation was chosen in this study, as it is in the region, which showed the highest aerodynamic loads on the individual row of collectors.

In the CFD simulations, 8 consecutive collectors were modelled in a single domain in order to simulate the solar field as shown in Figure 1. As the lateral boundaries were set to be periodic, the simulations emulated the interior collectors in a solar field with 8 rows of PTCs. These steady-state simulations were conducted using the Reynolds Average Navier–Stokes based Shear Stress Transport (SST) turbulence model (Menter, 1994). An individual parabolic trough had an aperture D of 5m, and a width of $2D$. The spacing between two rows was chosen as $2.8D$, a common layout for solar fields (Hosoya et al., 2008). The inlet condition was set to an atmospheric boundary layer flow according to category 2 as per Australian Standard (Standards Australia Limited/Standards

New Zealand, 2011). To achieve an adequate level of accuracy in the airflow around each trough a reasonably fine mesh is required, and the total number of mesh nodes is larger than 20M, which is the reason for performing these simulations in steady-state only.

A transient simulation is also conducted for the shallow trough. Initialised from the result of a single collector row in a steady state simulation, a short domain is simulated with a periodic inlet-outlet condition. A mass flow rate through the periodic interface was defined in accordance with the atmospheric boundary layer flow as above. The size of the trough and the row spacing are identical to the full field simulations mentioned above. These simulations have a significantly lower number of mesh nodes (ca 3M) and can therefore, with reasonable computational effort, be simulated in transient mode. The SST-SAS turbulence model (Menter and Egorov, 2010) was chosen for this simulation. While the transient simulation allows for an analysis of the time-dependent fluctuating effects of the wind, it represents the innermost troughs in the solar field only. The simulation setup as being periodic in both the lateral and the flow direction emulates an infinite field of collectors. A simulation time of 3 seconds was reached so far, and hence this simulation needs to be continued to allow for a more comprehensive analysis of the transient effects of the wind.

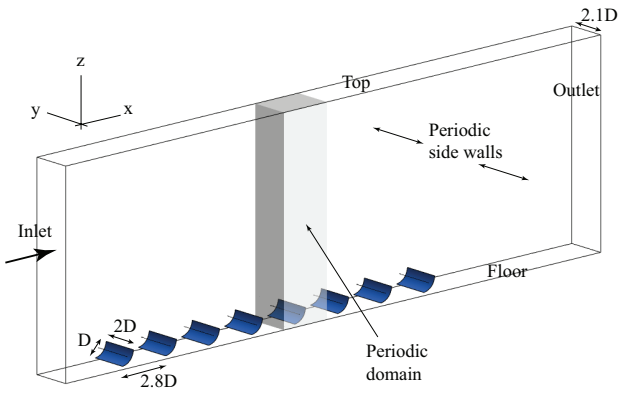

Figure 1. The domain of the solar field simulation with 8 rows of collectors. The grey area shows the size of the periodic domain.

The analysis of the data focuses on the flow fields along with the aerodynamic force coefficients (drag coefficient C_D, and lift coefficient $C_{L)}$, and the pitching moment coefficient C_M, which are determined as:

$$C_D = \frac{2F_D}{\rho V_\infty^2 A} \quad , \quad C_L = \frac{2F_L}{\rho V_\infty^2 A} \text{ , and } \quad C_M = \frac{2M_y}{\rho V_\infty^2 AD}$$

with the aerodynamic forces in the positive x and y directions, F_D and F_L, and the pitching moment M_y resulting from the the simulation. The free stream velocity V_∞ is set to 10m/s at a reference height of 3m, the density of air, ρ, is 1.185kg/m^3, and the characteristic area of the trough is $A = D \times 2D$.

With respect to the heat loss at the receiver tube, the average Nusselt number over the outer surface of the receiver is compared between the different trough geometries and positions. The Nusselt number (Nu) is defined as:

$$\mathrm{Nu} = \frac{hd}{k}$$

with the heat transfer coefficient $h = q/\Delta T$, the wall heat flux q determined by the simulation, the diameter of the receiver tube d being 0.1m, the thermal conductivity of air k = 0.026W/mK, and the temperature difference between surface and surrounding air, ΔT, being 75K.

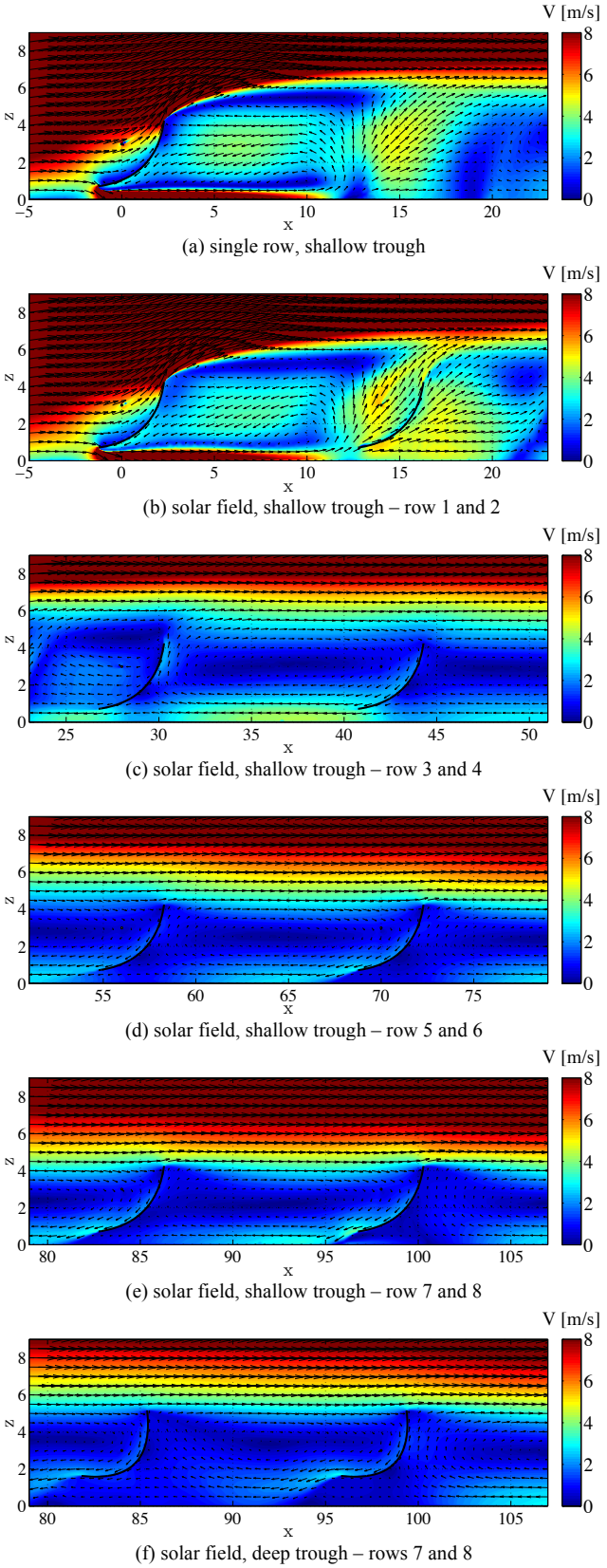

Figure 2. Contour of the velocity magnitude and velocity vectors around the shallow troughs: (a) single row, (b) – (e) solar field rows 1 through 8, and (f) the deep trough rows 7 and 8.

Results

Flow field analysis

Figure 2 shows the contour of the velocity magnitude around the shallow parabolic troughs along with velocity vectors for the simulated configurations in the central plane of the domain. For comparison, Figure 2 (a) shows the single row of the shallow trough, and the last two rows of the deep trough solar field are shown in Figure 2 (f). It can be seen that the flow around and behind the first row of the solar field simulation in (b) shows high similarity with the flow field around the single row in (a) up to about 2*D* behind the trough, while the backflow in the wake region is slightly stronger in the case of the single row. The angle at which the shear layer separates off the top edge of the trough, as well as the speed up effect underneath the trough, however, are almost identical between these two. The flow velocity around the receiver tube is slightly higher in the individual row than it is in the first row of the solar field.

In front of the second row the high-speed region that developed underneath the first row is turned upwards and leads to high velocities around the receiver tube. In Figure 2 (c) a small vortex in front of the top edge of the third row can be observed. The wake behind rows number 3 to 7 in (c) through (e) shows a significantly larger vortex forming, which extends over the entire space between two consecutive collector rows. As part of the wake a return flow close to the ground surface develops in front of the collector starting from row 3. The highest return velocity is reached at row 4, while it reduces further downwind, and it is almost stable from row 5 onwards.

From row 5 to row 6 in (d) the high-speed flow in the free stream flow lowers slightly closer to the top of the collector, which is likely still an effect of the initial separation at the trailing edge of the collector in the first row. The flow field in the wake behind rows number 6 and 7 seems almost identical. Behind the eighth collector row the wake is drawn closer to the ground, as no further collector follows.

For the deep trough, only a partial solar field is shown for brevity reasons. Due to the higher curvature of the deep trough, the angle of the separation at the first row is steeper than in the case of the shallow trough. Furthermore, the high velocity region underneath the trough extends further than the second row. Therefore, a constant flow field between two collector rows is only reached further downwind in the solar field. In a field of 8 rows of collectors this is not fully reached. A large vortex filling the space between two rows is reached only behind row 5, which is 2 rows later than for the shallow trough. This, together with the velocity field around rows 7 and 8 shown in Figure 2 (f), suggests that a steady flow field can be observed from about row 7 in a large solar field of deep troughs.

Drag and lift

The results of the solar field simulations for the aerodynamic loads confirm the observations from previous studies on wind loads in the solar field. A large drop of the absolute drag and lift coefficient shown in Figure 3 (a) and (b) is observed between rows 1 and 2. Further downwind there are still small, but noticeable changes of the coefficients, while from row 5 onwards the loads on the deep trough are virtually constant. In case of the shallow trough the changes beyond row 5 are minor, but the absolute values of both lift and drag are slowly growing. As in the simulations of a single row, also in the first row of the solar field the deep trough experiences higher lift and drag than the shallow trough. However, from row number 2 onwards this difference is minimised and is only minor in comparison with those in the first row. From row 5 onwards the difference in the aerodynamic forces on both the shallow and the deep trough is almost not existent. The deep trough even experiences slightly lower force coefficients than the shallow trough from row 6 onwards. The values of the drag and lift coefficient of the shallow trough approach those of the periodic simulation, however, they do not reach these values up to row 8. Hosoya et al. (2008) reported constant values for the aerodynamic loads from about row 5 onwards. Therefore, the data of the periodic simulation are shown for rows 5 through 8. Despite the different scale, and hence the significantly larger Reynolds number in the present study, the load coefficients resulting from the periodic simulation match closely with the experimental results reported by Hosoya et al. (2008) of 0.253 for the drag coefficient, and −0.167 for the lift coefficient. The results shown for the periodic simulation are averaged over 2 seconds simulation time, and the values of the forces and pitching moment showed signs of regularity. However, as the simulation time is still rather short, these results are only indicative at this stage.

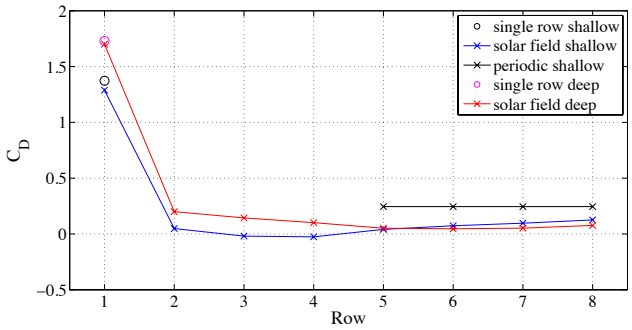

(a) drag coefficient

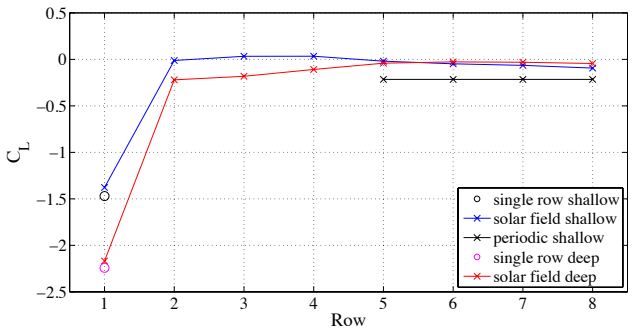

(b) lift coefficient

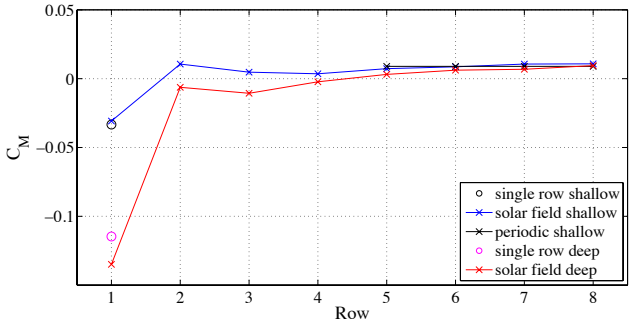

(c) pitching moment coefficient

Figure 3. The aerodynamic force and moment coefficients comparing the results of the solar field simulation of the shallow trough with those of the deep trough.

Pitching moment

The pitching moment shows a similar trend, as it reduces significantly in the downstream rows and converges towards a value of about 0.01 in the interior of the solar field for both the shallow and the deep trough. This value matches well with the result of the periodic simulations. It is also close to the value of 0.009 reported by Hosoya et al. (2008). In the single row the pitching moment coefficient is negative at a significantly higher absolute value for the deep trough than for the shallow one. This is also the case for the first row of the solar field.

Heat transfer

With respect to the heat transfer around the receiver tube the position of the trough in the solar field proves to only have a minor impact. As Figure 4 shows, the average Nusselt number in the case of the shallow trough is higher in the second row than in the first row and also in the individual row simulation. The combination of the wake and the strong upward flow in front of the trough of the second row have a strong effect on the heat loss in the receiver tube. In the following rows, however, the variations are relatively small and the Nusselt number drops back to a value lower than the one observed in the first row. From row 6 onwards the Nusselt number slowly rises again. For the deep trough the peak Nusselt number also occurs in the second row, and a rising Nusselt number is observed from row 4 onwards. Except for row 2, where the peak is similarly high for both geometries, the average Nusselt number is significantly lower in case of the deep trough than it is for the shallow trough. The average Nusselt number from the periodic simulation is not shown, as it showed high non-regular fluctuations at the time of writing, which are expected to become more regular with progressing simulation time.

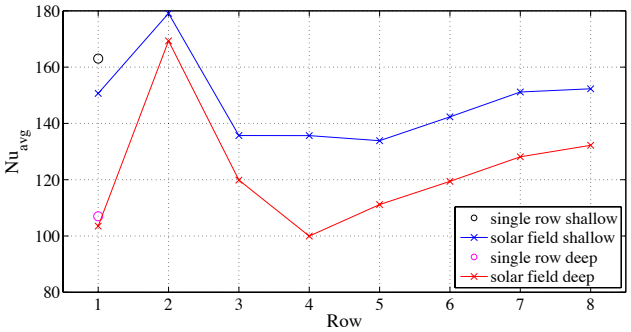

Figure 4. The average Nusselt number at the receiver surface comparing the results of the solar field simulation of the shallow trough with those of the deep trough.

Discussion and Conclusions

This study shows the effects of the wind on a full-scale field of parabolic trough collectors. The velocity fields around the solar fields with two different trough geometries are analysed and compared. A constant flow field is reached at row number 5 for a field of shallow troughs, and roughly 2 rows further downwind for a field of deep troughs.

The lift and drag forces acting on the collectors are dramatically reduced already in the second row of the solar field and reach a stable value around row number 5 in the case of the deep troughs. For the shallow troughs the forces still experience a slight increase beyond this point, while still remaining at a low value. The downstream collectors also experience significantly lower pitching moments than the first collector row. The heat loss at the surface of the receiver tube only experiences major changes in rows 2 and 3, and settles for a value close to that of row 1 afterwards.

While the deep trough is subjected to higher loads than the shallow one on the level of an individual row of collectors, the force and moment coefficients in the solar field are almost identical with those of the shallow trough downwind of row 4. In the entire solar field the thermal losses due to forced convection are significantly lower for the deep trough than for the shallow trough. These results suggest that a field of deep troughs could be advantageous over a shallow collector field. Alternatively a field with mixed collector geometries to optimise the plant performance both at the edges as well as in the interior of the solar field could prove to be beneficial.

The transient effects in the solar field play an important role in the turbulent regions of the wake, and hence they affect the aerodynamic loads on the interior collectors. Therefore, the next step in this research is to continue the transient simulations of the deep interior collectors by means of a periodic simulation of a single row in order to capture not only the mean loads and also the peak forces and moments affecting the troughs. Furthermore, alterations of the trough geometry are planned to be tested in solar field simulations with the aim to reduce loads further, especially in the most upwind rows. A confirmation of the stable flow field and load coefficient downwind of row 5-6 could be obtained by using an even larger domain with 10 or more collector rows.

References

Hachicha A, Rodríguez I, Castro J, Oliva A (2013) Numerical simulation of wind flow around a parabolic trough solar collector, Applied Energy 107:426–437

Hosoya N, Peterka J, Gee RC, Kearney DW (2008) Wind tunnel tests of parabolic trough solar collectors wind tunnel tests of parabolic trough solar collectors. Tech. rep., National Renewable Energy Laboratory, Golden, Colorado, USA

Menter FR (1994) Two-equation eddy-viscosity turbulence models for engineering applications, AIAA Journal 32(8):1598–1605

Menter FR, Egorov Y (2010) The scale-adaptive simulation method for unsteady turbulent flow predictions. Part 1: Theory and model description, Flow, Turbulence and Combustion 85(1):113–138

Mier-Torrecilla M, Herrera E, Doblaré M (2014) Numerical Calculation of Wind Loads over Solar Collectors, Energy Procedia 49:163–173

Naeeni N, Yaghoubi M (2007) Analysis of wind flow around a parabolic collector (1) fluid flow, Renewable Energy 32(11):1898–1916

Paetzold J, Cochard S, Vassallo A, Fletcher DF (2014) Wind engineering analysis of parabolic trough solar collectors: The effects of varying the trough depth, Journal of Wind Engineering and Industrial Aerodynamics 135:118-128

Peterka, J, Sinou, J, Cermak, J (1980) Mean wind forces on parabolic-trough solar collector, Tech. rep., Sandia Laboratories, Albuquerque, New Mexico, USA

Standards Australia Limited/Standards New Zealand (2011) AS/NZS 1170.2:2011 Structural design actions - Part 2: Wind actions

Sun H, Gong B, Yao Q (2014) A review of wind loads on heliostats and trough collectors, Renewable and Sustainable Energy Reviews 32:206–221